Available online at www.sciencedirect.com
SCIENCE DIRECT®
International Journal of Multiphase Flow 30 (2004) 1093–1119
International Journal of Multiphase Flow
www.elsevier.com/locate/ijmulflow

Flow characteristics in hydraulically equilibrium two-phase flows in a vertical 2×3 rod bundle channel

M. Sadatomi, A. Kawahara *, K. Kano, S. Tanoue

Department of Mechanical Engineering and Materials Science, Kumamoto University, Kurokami 2-39-1, Kumamoto City 860-8555, Japan

Received 29 February 2004; received in revised form 20 May 2004

Abstract

In order to increase data on two-phase flow distribution in a multi-subchannel system, being similar to a rod bundle, experiments have been carried out using water and air at ambient pressure and temperature as the working fluids and a newly constructed 2×3 rod bundle channel as the test channel. The channel contained six rods in rectangular array and two-kinds of six subchannels, simulating a BWR fuel rod bundle. Experimental data on flow distribution and pressure drop along each subchannel axis were obtained in various single- and two-phase flows under a hydraulic equilibrium flow condition. From the measured pressure drop in the single-phase flow, friction factor data in each subchannel were obtained. The two-phase pressure drop data were compared with calculations by a simple, one-dimensional, one-pressure two-fluid model. In addition, Taylor bubble velocity in each subchannel in slug-churn flows was measured with a double needle contact probe. Using the bubble velocity data, we obtained a subchannel void fraction in each subchannel, and discussed a relationship of the subchannel void fractions between two different subchannels. Results of such experiments and discussions are presented in this paper.

Keywords: Subchannel analysis; Rod bundle; Hydrodynamic equilibrium flow; Flow distribution; Pressure drop; Taylor bubble velocity; Void fraction distribution

* Corresponding author. Tel./fax: +81 96 342 3753.
E-mail address: akimaro@mech.kumamoto-u.ac.jp (A. Kawahara).

0301-9322/$ - see front matter © 2004 Elsevier Ltd. All rights reserved.
doi:10.1016/j.ijmultiphaseflow.2004.05.012

1. Introduction

In the prediction of thermal-hydraulic behavior of a coolant in a BWR fuel rod bundle by a subchannel analysis, it is necessary to evaluate accurately fluid transfer between subchannels (Lahey and Moody, 1993; Ninokata et al., 1997). The fluid transfer in the gas–liquid two-phase flow consists of three independent components; void drift, diversion cross-flow and turbulent mixing (Lahey and Moody, 1993; Sadatomi et al., 1994; Sato et al., 1996; Sadatomi et al., 1997). Of the three, the turbulent mixing alone exists in a hydraulically equilibrium flow, in which mass and volume of each phase do not move between subchannels as a time averaged value. In a non-equilibrium flow, on the other side, the three components coexist and mass and volume of each phase move between subchannels. As for the respective components, however, no decisive prediction model has been obtained yet, so the modeling is still continuing (e.g., Ninokata et al., 1997; Carlucci et al., 2004).

In order to evaluate net transfer of gas phase mass flux from subchannel i to j due to the void drift, $\dot{m}_{Gij}$, the following void settling model (Gonzalez-Santalo and Griffith, 1972; Lahey and Moody, 1993) has been widely used (e.g., Kazimi and Kelly, 1983; Tapucu et al., 1994; Ninokata et al., 1997),

$$\dot{m}_{Gij} = \rho_G \widetilde{D}[(\varepsilon_i - \varepsilon_j) - (\varepsilon_i - \varepsilon_j)_{EQ}]/S_{ij}, \tag{1}$$

where ρ_G is the gas phase density, $\widetilde{D}$ the void diffusion coefficient, $(\varepsilon_i - \varepsilon_j)$ the void fraction difference between subchannels, and S_{ij} the gap clearance between subchannels. The subscript 'EQ' denotes the hydrodynamic equilibrium state. The validity of Eq. (1) was confirmed by Sadatomi et al. (1994, 1996a) and Kawahara and Sadatomi (2000a,b) when experimental values of $\widetilde{D}$ and $(\varepsilon_i - \varepsilon_j)_{EQ}$ were given as input data. Thus, for prediction of the void drift in a non-equilibrium flow, it is essential to predict accurately the flow and the void fraction distributions in the equilibrium flow. Even in the equilibrium flow, however, there is no versatile prediction method at the present time.

Gonzalez-Santalo and Griffith (1972), Sato et al. (1987, 1988), Sadatomi et al. (1994) performed experiments to obtain data on air–water two-phase flow distributions in an equilibrium flows in a channel made up of two different subchannels, i.e., a two-subchannel system. Such experiments using geometrically simpler channel is superior to rod bundle experiments if we want to see phenomena more clearly and to obtain a lot of reliable data covering wide range of flow condition. However, we should are worry about whether a lot of the knowledge derived from experiments using a two-subchannel system for the equilibrium flows as well as the non-equilibrium flows (Rowe and Angle, 1969; Gonzalez-Santalo and Griffith, 1972; Rudzinski et al., 1972; Tapucu et al., 1988, 1990; Sato et al., 1987, 1988, 1996; Teyssedou et al., 1989a,b; Sadatomi et al., 1994, 1995, 1996a,b, 1997; Kawahara et al., 1997, 2000a,b,c) are applicable to the prediction of the flow and the void fraction distributions in a mutli-subchannel system, which is close to a BWR fuel element. In addition, for inclusive validation of a subchannel analysis code, data in a multi-subchannel system are indispensable.

Regarding a multi-subchannel system, Lahey et al. (1972) measured corss-sectional distributions of quality and mass flux in a 3×3 rod bundle subchannels under the equilibrium flow con-

ditions, using steam and water as the working fluids. A decade later, Sterner and Lahey (1983) obtained data on the lateral distributions of quality and mass flux in a 2×2 rod bundle subchannels, using air and water. Yadigaroglu and Maganas (1995) measured also the distributions of quality and mass flux for fully developed Refrigerant-114 two-phase flows in a three-subchannel test section, being geometrically similar to corner, side and center subchannels of a BWR. All the studies mentioned above are useful to validate various subchannel analysis codes. However, the data on the flow distributions have been limited, and no data have been obtained on inter-subchannel fluids transfers, e.g., turbulent mixing rates, necessary in a subchannel analysis. Thus, there is a strong demand to broaden the database with both the flow distribution and the inter-subchannel fluids transfer to validate fluids transfer models as well as subchannel analysis codes so far proposed.

Therefore, we have carried out an experimental program to get database for a multi-subchannel system. In the program, a vertical test channel, having symmetric two kinds of six subchannels around 2×3 square array rods, was newly constructed, as shown in Fig. 1 (Sadatomi et al., 2004). Using this channel, we measured single-phase liquid and two-phase gas–liquid turbulent mixing rates for hydraulically equilibrium flows over relatively wide flow conditions (Sadatomi et al., 2004). Following to the turbulent mixing experiment, experiments in this study were performed also for hydraulically equilibrium flows to obtain data on flow distribution for water single-phase flow and air–water two-phase flow. In this paper, flow distribution data are presented for various two-phase flows, covering bubble, slug, churn and annular flow regimes. Besides the flow distribution, pressure drop along each subchannel axis was also measured. From the measured pressure drop in the single-phase flow, friction factor data in each subchannel were obtained. The two-phase pressure drop data were compared with calculations by a simple, one-dimensional, one pressure two-fluid model. In addition, Taylor bubble velocity in each subchannel in slug or churn flow was measured with a double needle contact probes. Using the bubble velocity data, we obtained data on a void fraction in each subchannel. The void fraction data were used to examine existing subchannel void fraction relationships (Lahey et al., 1972; Carlucci et al., 2004) proposed for hydraulic equilibrium flows. We present results of the above experiments, comparisons and examinations.

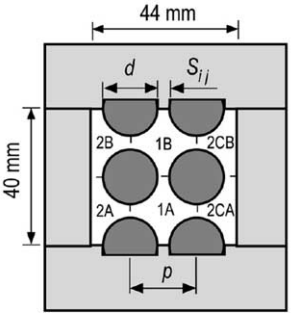

Rod diameter: d = 16 mm
Rod pitch: p = 20 mm
Pitch to diameter ratio: p/d = 1.25
Gap clearances: $S_{11} = S_{12} = S_{22}$ = 4 mm

		Ch.1	Ch.2	Whole
Hydraulic diameter	mm	14.3	11.2	12.3
Flow area	mm^2	194	138	941

Fig. 1. Cross-sectional geometry and dimensions of the test channel.

2. Experiment

2.1. Test channel and test rig

Cross-section of the test channel in this study is illustrated in Fig. 1. The channel is the same as that used in our previous study (Sadatomi et al., 2004). The channel is designed so as to simulate a BWR fuel rod bundle channel and referred to as 2×3 rod bundle channel in our laboratory. This channel consisted of transparent acrylic rectangular duct, two brass rods placed in the central part of the duct and four semi-circular acrylic rods on the duct walls face each other. To suppress vibration of the rod, the outer diameter of the rod was 16 mm, about 3.5 mm larger than that of a BWR rod. The gap clearances between the two rods as well as the rod and the duct wall were 4.0 mm. As mentioned in Introduction, the purpose of this study is to get a database consisting of both the two-phase flow distribution and the turbulent mixing rates between the respective subchannels in a multi-subchannel system. However, it seems difficult to obtain the turbulent mixing rates data in an actual BWR channel geometry. In the BWR, at least four kinds of turbulent mixing for each phase appear, i.e., the mixings between corner-side, side-side, side-center and center-center, but the determination of them at once seems impossible as far as we know (Sadatomi et al., 2004). Therefore, we omitted the corner subchannel and simplified the channel into the present 2×3 rod bundle channel, which is a rod bundle consisting of symmetric two kinds of six subchannels by considering the easiness in both setting inlet flow rates in each subchannel and acquiring the data on turbulent mixing rates between the respective subchannels. The six subchannels are the two central subchannels and the four wall subchannels, respectively called as Ch. 1 (=Ch. 1A=Ch. 1B), Ch. 2 (=Ch. 2A=Ch. 2B=Ch. 2CA=Ch. 2CB). The hydraulic diameters of Ch. 1, Ch. 2 and the whole chanel were 14.3, 11.2 and 12.3 mm, and the cross-sectional areas of them were 194, 138 and 941 mm^2, respectively.

An essential part of the test rig is illustrated in Fig. 2. The test channel was divided into three sections, entry (2.0 m in length), test (2.25 m) and discharge sections (0.5 m), from the bottom to the top. At the entry section, by considering the symmetry of the cross-section, six subchannels were grouped into three by four 1 mm thick partitions as shown in Fig. 3A, and introduced air and water in the two side subchannel groups at the same flow rates. The flow rates of air and water introduced in the respective subchannel groups were measured with calibrated rotameters and turbine flow meters. At the test section, no partition exists in every gap between the rods, so that inter-subchannel fluid transfer could occur through all the gaps. In this section, a system pressure and axial pressure drops in the respective subchannels were measured with a pressure transducer and differential pressure transducers, respectively. At the discharge section, six subchannels were grouped into another three as shown in Fig. 3C. In order to realize isokinetic discharge form the test section, the pressure difference among the three groups was minimized at the inlet of the discharge section for monitoring the symmetry of the flow between subchannel groups 12A and 12B. This was done by controlling the openings of the respective air discharge valves connected to three separator rooms. The flow rate of separated air in each subchannel group was measured with a calibrated wet gas meter or the turbine flow meter, the flow rate of water with a metering tank.

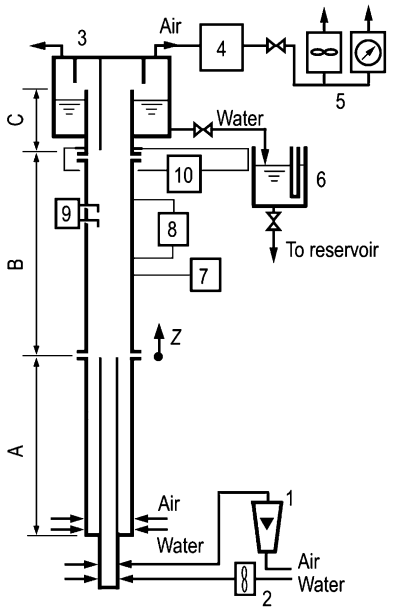

1. Rotameter
2. Turbine flow meter
3. Separator
4. Surge tank
5. Gas flow meter
6. Metering tank
7. Pressure transducer
8. Differential pressure transducer
9. Needle contact probes
10. DP transducer for monitoring cross-sectional pressure difference

Name of section	Length m
A Entry section	2.0
B Test section	2.25
C Discharge section	0.5

Fig. 2. Test rig.

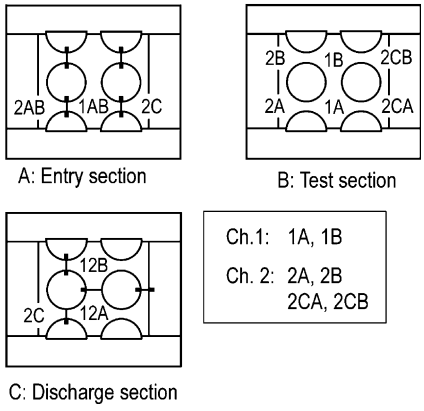

Fig. 3. Cross-sectional view of each section in the test rig.

2.2. Determination of subchannel flow rates at channel outlet

When making use of the geometrical symmetry of the test channel, we determined the flow rates of k-phase ($k = \mathrm{G}$ for gas phase, $k = \mathrm{L}$ for liquid phase) in the respective subchannels, $Q_{k1\mathrm{A}}$, $Q_{k1\mathrm{B}}$ and Q_{k2}, from the following continuity relations,

$$Q_{k1\mathrm{A}} = Q_{k12\mathrm{A}} - \frac{Q_{k2\mathrm{C}}}{2}, \quad Q_{k1\mathrm{B}} = Q_{k12\mathrm{B}} - \frac{Q_{k2\mathrm{C}}}{2}, \quad Q_{k2} = \frac{Q_{k2\mathrm{C}}}{2}, \tag{2}$$

where Q_{k12A}, Q_{k12B} and Q_{k2C} are the flow rates measured in the respective subchannel groups 12A, 12B and 2C at the outlet.

2.3. Setting hydrodynamic equilibrium flow

Equilibrium flow is such a flow that the mass flow rates of both phases in every subchannel do not vary along the channel axis. Equilibrium flow does appear at a midstream of the test section irrespective of the inlet flow distribution if the test section were very long. In the present test channel, however, the length of the test section is 2.25 m, and is insufficient for the equilibrium flow to appear. Therefore, we employed the following try-and-error method to realize the equilibrium flow.

(1) As a first trial, at the test section inlet, we introduced air and water into the three subchannel groups so that the ratio of the flow rate of k-phase in each group to the whole channel, say, $Q_{k1AB}(0)/Q_k$, is equal to the ratio of cross-sectional area in the corresponding group, A_{1AB}/A.
(2) At the test section outlet, we measured the flow rate of k-phase in each subchannel group, say Q_{k12A}, and calculated the flow rate ratio which have to be feedbacked to the inlet.
(3) According to the calculation result from (i) and (ii), the inlet flow rates in the respective subchannel groups were changed. After that, the flow rates of both phases in the whole channel were checked to be the same as those in the first step.

This procedure was iterated until the ratio of flow rate at the test section inlet and the outlet was sufficiently close in each subchannel. Finally, when these ratios became close enough (within ±1%), we adopted these ratios as those for the hydrodynamic equilibrium flow. In order to obtain the equilibrium ratios, three to six iterations were required depending on the given flow condition.

2.4. Measurement of Taylor bubble velocity in each subchannel

Taylor bubble velocity in each subchannel was measured with a double needle-contact probe. The paired probes 12.0 mm apart were placed in each subchannel at a cross-section 1550 mm downstream from the test section inlet as shown in Fig. 2. The tip of the probe was set at the centroid of the subchannel. Signals from the paired probes were fed into an FFT analyzer to calculate cross-correlation and to determine the mean delay time of these signals, $\Delta\tau$. Taylor bubble velocity in slug and churn flows, $u_{Gi,exp}$, was calculated from

$$u_{Gi,exp} = \frac{l_p}{\Delta\tau}, \tag{3}$$

where l_p is the distance between the two tips.

2.5. Flow conditions

The working fluids were water and air at atmospheric pressure and at room temperature. Fig. 4 shows flow conditions. The ordinate and the abscissa indicate respectively the volumetric fluxes of

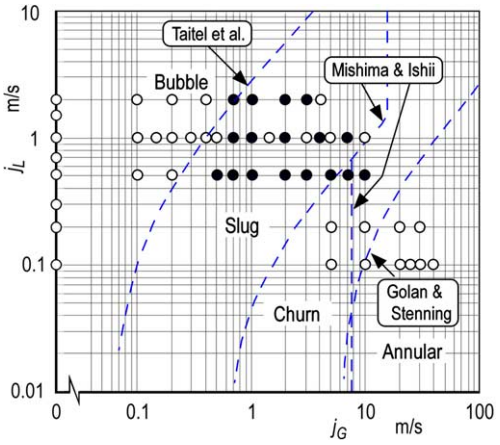

Fig. 4. Flow conditions (solid or open symbol: with or without Taylor bubble velocity measurement).

liquid and gas phases in the channel as a whole. For reference sake, flow pattern boundaries determined from the correlations of Taitel et al. (1980), Mishima and Ishii (1984) and Golan and Stenning (1969) are drawn as broken curves. The measurement of the flow distribution was made at all the flow conditions marked with open and solid symbols, and the measurements of Taylor bubble velocity were made at condition with solid symbol alone. In the single-phase flow experiments, the range of the mean water velocity was 0.1–2.0 m/s. In the two-phase flow experiments, on the other side, flow condition covered were as follows: the range of the water volumetric flux was 0.1–2.0 m/s; that of air was 0.1–40 m/s; that of void fraction in the whole channel was 0.07–0.98, which was calculated by Chisholm's correlation (1973). Flow patterns covered were bubble, slug, churn and annular flows.

3. Results and discussions

3.1. Single-phase water flow distribution

Fig. 5 shows data on flow distribution in single-phase water flows. The ordinate is the ratio of the water volume flow rate in one subchannel to that in the whole channel, Q_{Li}/Q_L. The abscissa is the Reynolds number defined as

$$Re = \frac{\rho_L u_L D_h}{\mu_L}, \tag{4}$$

where u_L and D_h are the mean axial velocity and the hydraulic diameter in the whole channel. In the present experiment, the range of u_L was 0.1–2.0 m/s, and that of Re 1.3×10^3 to 2.6×10^4. Q_{L1}/Q_L is the averaged value of two Ch. 1, i.e., Ch. 1A and Ch. 1B, and Q_{L2}/Q_L the averaged value of four Ch. 2. The ratio of cross-sectional area in one subchannel to the whole channel, A_i/A is also indicated. The measured values of Q_{Li}/Q_L in laminar and turbulent flow regimes are nearly

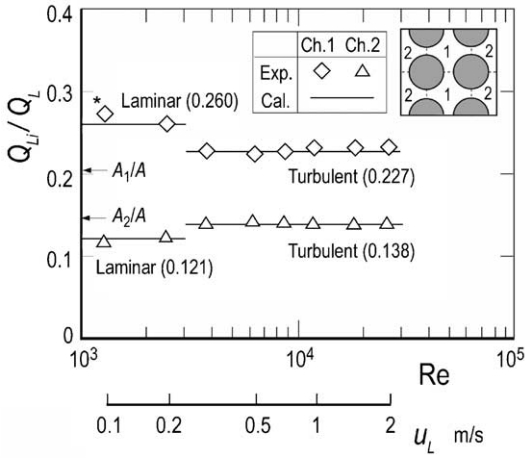

Fig. 5. Flow distribution data in hydraulically equilibrium single-phase water flows.

constant in the respective regimes, and agree well with the calculation lines by the following Sato et al.'s equation (1983),

$$\frac{Q_i}{Q} = \frac{A_i}{A}\left(\frac{C}{C_i}\right)^{\frac{1}{2+n}}\left(\frac{D_{hi}}{D_h}\right)^{\frac{1-n}{2+n}}, \tag{5}$$

$$C = \left[\sum_i^k \left(\frac{A_i}{A}\right)\left(\frac{1}{C_i}\right)^{\frac{1}{2+n}}\left(\frac{D_{hi}}{D_h}\right)^{\frac{1-n}{2+n}}\right]^{-(2+n)}. \tag{6}$$

Eqs. (5) and (6) were derived from a continuity equation and the equation of equal-pressure-gradient between subchannels. In Eqs. (5) and (6), n and C_i are the power and the geometry factor of the following friction factor-Reynolds number relationship.

$$\lambda_i = C_i Re_i^n. \tag{7}$$

Here, λ_i is the Darcy's friction factor for Ch. i, $C_i = C_{li}$ for laminar flow and $C_i = C_{ti}$ for turbulent flow, and $n = -1$ for laminar flow and $n = -0.25$ for turbulent flow. According to Rehme's study (1973) on C_{li} of laminar flow in a rod bundle, $C_{li} = 90.4$ and 88.7 for Ch. 1 and Ch. 2 in the present channel. C_{ti} for turbulent flow can be estimated from Sadatomi et al.'s correlation (1982)

$$\frac{C_{ti}}{C_{t0}} = \sqrt[3]{0.0154\frac{C_{li}}{C_{l0}} - 0.012} + 0.85. \tag{8}$$

Here, C_{t0} and C_{l0} are the geometry factors for a circular channel, being $C_{t0} = 0.316$ and $C_{l0} = 64$. The agreement between the data and the calculations is excellent except for the data point asterisked, which probably have a relatively large measurement error because of the extremely small water flow rate.

3.2. Two-phase gas–liquid flow distribution

Fig. 6 shows data on the gas and the liquid flow distributions for two-phase bubble, slug and churn flows at $j_L = 1.0$ m/s under hydraulically equilibrium flow conditions. The ordinate indicates the ratio of volume flow rate in one subchannel to the whole channel, Q_{ki}/Q_k for each phase ($k = G$ for gas phase or $k = L$ for liquid phase). The abscissa indicates the volumetric flux of the gas phase for the whole channel, j_G. Data points are labeled according to both the fluid and subchannel. For reference sake, the ratio of the cross-sectional area, A_i/A, and the wetted perimeter, L_i/L, are also shown. The broken line represents the flow rate ratio for the single-phase turbulent flow mentioned in Section 3.1. If two-phase mixture were homogenous, the data points would be on the line. In order to confirm symmetry of the flow between Ch. 1A and Ch. 1B, the data in these subchannels are plotted. The agreement of these data is within ±1.3% for liquid phase and ±6.5% for gas phase, thus we can confirm the symmetry. In the subsequent Figs. 7 and 8, therefore, the flow rate ratio averaged between Ch. 1A and Ch. 1B alone will be presented for simplicity. In Fig. 6, the flow rate ratios of the gas and the liquid are higher in Ch. 1 than Ch. 2, because the cross-sectional area is larger in Ch. 1. In bubble flow, the flow rate ratios of both phases were close to the values in the single-phase turbulent flow. At bubble flow to slug flow transition, the ratio of the liquid phase, Q_{Li}/Q_L, does not change so much, but that of the gas phase, Q_{Gi}/Q_G, drastically changes: the ratio in Ch. 1 increases up to 1.5 times of that in the single-phase turbulent flow, while that in Ch. 2 decreases. The probable reason is that Taylor bubbles in slug flow are apt to flow in Ch. 1 rather than Ch. 2 because the cross-sectional area in Ch. 1 is larger than that in Ch. 2. In slug or churn flow, the flow rate ratio of the gas phase in Ch. 1 shows a peak value at $j_G = 3.0$ m/s. After that, the ratio in Ch. 1 decreases with increasing of j_G, while that in Ch. 2 increases. With further increase in j_G, the flow pattern becomes closer to annular flow, and the

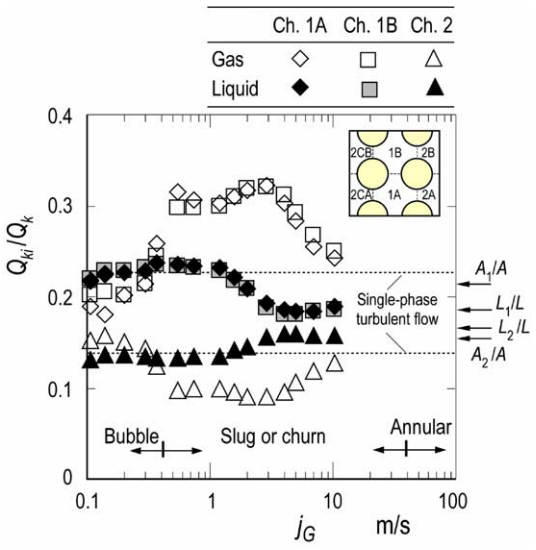

Fig. 6. Gas and liquid flow distribution data in hydraulically equilibrium two-phase bubble, slug and churn flows at $j_L = 1.0$ m/s.

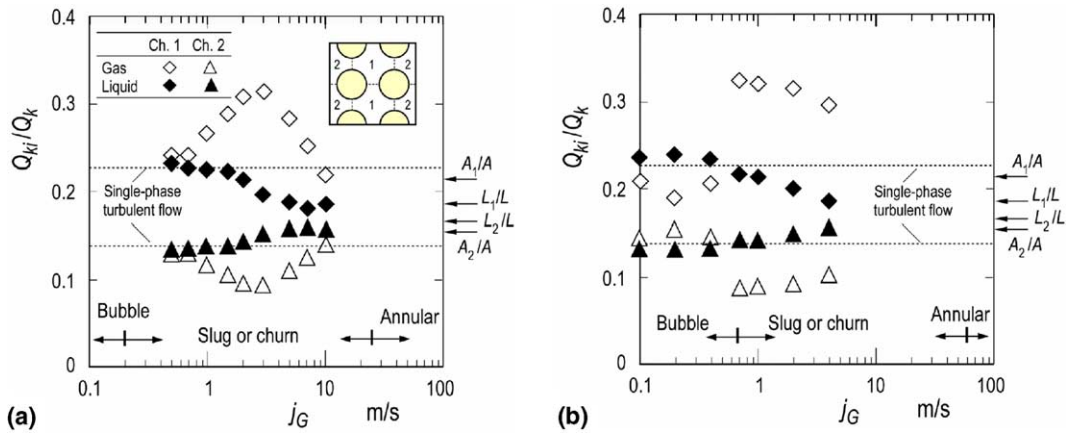

Fig. 7. Gas and liquid flow distribution data in hydraulically equilibrium two-phase bubble, slug and churn flows at: (a) $j_L = 0.5$ m/s and (b) $j_L = 2.0$ m/s.

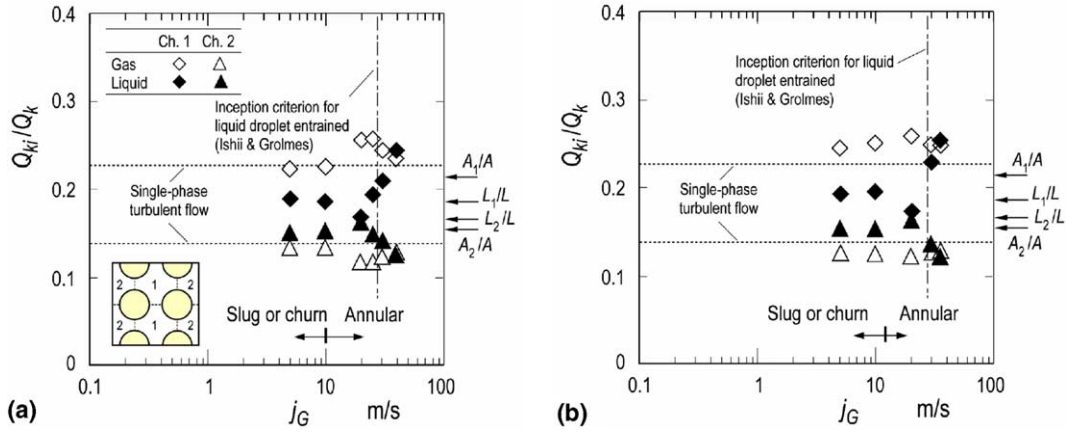

Fig. 8. Gas and liquid flow distribution data in hydraulically equilibrium two-phase annular flows at: (a) $j_L = 0.1$ m/s and (b) $j_L = 0.2$ m/s.

ratio of the gas phase seems to approach the calculated value in the single-phase turbulent flow again.

Fig. 7(a) and (b) show data on the flow distributions at $j_L = 0.5$ and 2.0 m/s. The trends of data in these figures are similar to that at $j_L = 1.0$ m/s.

Fig. 8(a) and (b) show the flow distribution data in churn and annular flows at $j_L = 0.1$ and 0.2 m/s, respectively. In annular flow region, the inception criterion for liquid droplet entrainment by Ishii and Grolmes (1975) are shown to determine the effects of liquid droplet in the gas core. Non-uniform flow distributions, different from the single-phase turbulent flow distribution, are also seen in annular flow region, though the degree of the non-uniformity is smaller than that in slug or churn flow region of Figs. 6 and 7. In Fig. 8(a) and (b), the non-uniformity mainly depends on

j_G in the present flow rates conditions. With increasing of j_G, the gas flow rate ratio, Q_{Gi}/Q_G, in annular flows tends to approach that in the single-phase turbulent flow. The liquid flow rate ratio, Q_{Li}/Q_L, on the other side, is close to the ratio of L_i/L when $j_G < 25$ m/s. With further increasing of j_G, however, the Q_{Li}/Q_L becomes close to the ratio for the single-phase turbulent flow. The probable reason of this change in Q_{Li}/Q_L is as follows: In lower j_G region, almost all the liquid flows as the liquid film on the channel wall and the film thickness is almost uniform along the channel periphery, thus $Q_{Li}/Q_L \approx L_i/L$. In higher j_G region, on the other side, some parts of the liquid might entrain into the gas core. The liquid entrainment fraction in the gas core usually increases with j_G, and the liquid film thickness becomes thinner, thus the flow approaches homogenous flow of gas with fine liquid entrainments, i.e., $Q_{Li}/Q_L \approx$ the ratio for the single-phase turbulent flow. According to the inception criterion by Ishii and Grolmes (1975), the gas core might contain liquid droplets if $j_G > 28$ m/s in the present flow condition.

As described above, the flow distribution data in the present six-subchannel system depend strongly on the two-phase flow pattern. A similar dependency had been confirmed in a two-subchannel system (Gonzalez-Santalo and Griffith, 1972; Sato et al., 1987, 1988; Sadatomi et al., 1994). These results suggest that there is a similarity in the mechanism governing the flow distribution between these two systems. Accordingly, a lot of knowledge obtained in a two-subchannel system must be applicable for the prediction of the flow distribution in a multi-subchannel system.

3.3. Pressure drop in each subchannel for single-phase and two-phase flows

Experimental data on the subchannel friction factor, λ_i, in hydraulic equilibrium single-phase water flows were obtained by substituting experimental data of the axial pressure gradient, $(\Delta P/\Delta Z)_i$, and the mean water velocity in the subchannel, u_{Li}, into the next equation

$$\lambda_i = \left(\frac{\Delta P}{\Delta Z}\right)_i \frac{2D_{hi}}{\rho_L u_{Li}^2}. \tag{9}$$

Here, ρ_L is the liquid density. The results of λ_i are plotted against the subchannel Reynolds number, Re_i $(=\rho_L D_{hi} u_i/\mu_L)$, in Fig. 9(a) and (b), respectively for the larger subchannels, Ch. 1A and Ch. 1B, and the smaller ones, Ch. 2A, Ch. 2B, Ch. 2CA and Ch. 2CB. Solid lines are the calculations of the friction factor for the respective subchannels by Rehme's method (1973) for laminar flow and Sadatomi et al.'s equation (1982) for turbulent flow. In addition, broken lines are those for circular pipe, i.e., by Hagen–Poiseuille equation for laminar flow and Blasius' equation for turbulent flow. The friction factor data agree with the calculations by Sadatomi et al.'s equation rather than Blasius' equation for a fully developed turbulent flow region. Sadatomi et al.'s equation is, therefore, more useful as a constitutive equation of λ_i, needed in a subchannel analysis code for prediction of the flow distribution, the pressure drop, etc., in a fuel rod bundle.

Fig. 10 shows the axial pressure gradient measured under the equilibrium two-phase flow conditions. The ordinate is the pressure gradient in Ch. i, $(dP_i/dZ)_i$, and the abscissa the superficial gas velocity in the whole channel, j_G. Since the pressure gradient agreed within ±6% in every subchannel, the mean value between Ch. 1 and Ch. 2 is plotted. From this agreement, we reconfirmed that the flow measured in the 2×3 rod bundle channel was an equilibrium flow. The general trend of the data is that the pressure gradient increases with j_L, but does not necessarily with j_G, especially at $0.2 < j_G < 2$ m/s.

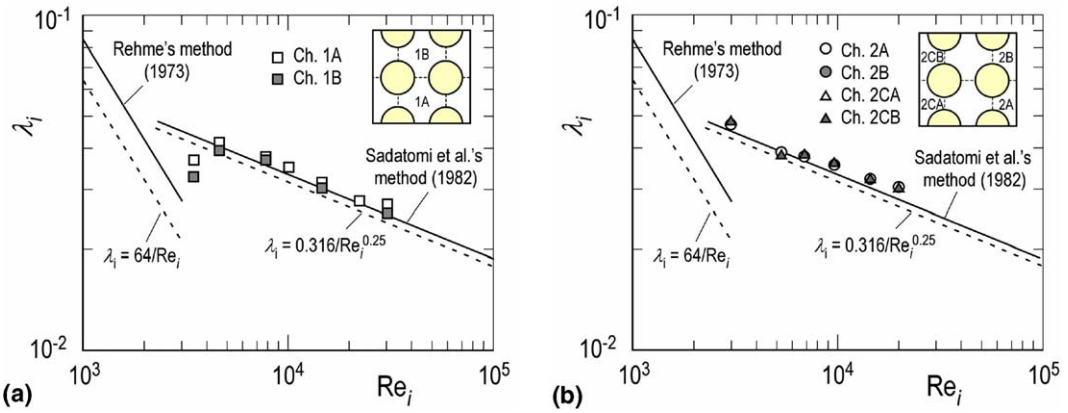

Fig. 9. Friction factor and Reynolds number relationship for single-phase water flow in the 2×3 rod bundle channel: (a) data for larger subchannel, Ch. 1A and Ch. 1B, and (b) data for smaller subchannel, Ch. 2A, Ch. 2B, Ch. 2CA and Ch. 2CB.

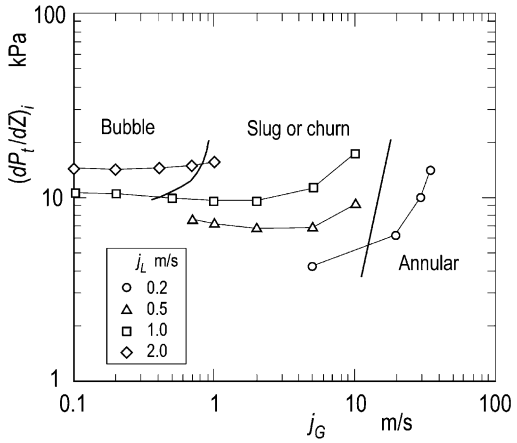

Fig. 10. Pressure gradient in a subchannel for hydraulically equilibrium two-phase flows in the 2×3 rod bundle channel.

A subchannel analysis code was tested against the two-phase pressure drop data mentioned above. The code is based on a simple, one-dimensional, two-phase two-fluid model, and consists of simultaneous equations of the axial momentums for both phases. In the calculation, the flow rates of both phases in each subchannel are given as input data, and a one-pressure model was adopted because the flow under consideration is a vertical flow. For closing the momentum equations, constitutive equations expressing the interfacial friction force between gas and liquid as well as the wall friction force between fluids and walls of channel and rod are required, but no decisive equation exists. So, the following correlations were tested for the interfacial friction correlation:

/Correlations in TRAC-PF1/MOD1 code (Lies et al., 1988);
/Correlations in RELAP5/MOD3 code (Carlson et al., 1990);

/Fukano and Furukawa (1998) for annular flow;
/Henstock and Hanratty (1976) for annular flow;
/Moeck and Stachiewitz (1970) for annular flow;
/Wallis (1969, 1970) for annular flow;

and the wall friction for liquid phase:

/Correlation in TRAC-PF1/MOD1 code (Lies et al., 1988);
/Correlation in RELAP5/MOD3 code (Carlson et al., 1990);
/Separated flow model (Chierici et al., 1974; Ali et al., 1993).

Regarding the wall friction for gas phase, it was taken as zero because the channel wall was wetted by water in the present experimental range. In the separated flow model, the wall friction force per unit volume, F_{WL}, is calculated from

$$F_{WL} = \lambda_{TPi} \frac{1}{D_{hi}} \frac{\rho_L u_{Li}}{2}. \tag{10}$$

Here, u_{Li} is the mean liquid velocity ($=j_{Li}/(1-\varepsilon_i)$). The two-phase friction factor, λ_{TPi}, is evaluated from

$$\lambda_{TPi} = C_i Re_{TPLi}^n, \tag{11}$$

$$Re_{TPLi} = \rho_L u_{Li} D_{hi}/\mu_L. \tag{12}$$

Here, the calculation methods of C_i and n was described in Section 3.1.

Fig. 11(a) and (b) show comparisons of the pressure gradient between experiment and calculation by (a) TRAC-PF1/MOD1 code and (b) RELAP5/MOD3 code for evaluating the wall and the interfacial friction forces. It is clear that the predictability of the correlations is superior in TRAC-PF1/MOD1 than RELAP5/MOD3, though the predictability is not sufficient. It is also interesting that the prediction with TRAC-PF1/MOD1's correlation under-predicts most of the present data, while that with RELAP5/MOD3's one over-predicts. In addition, some data are out of Fig. 11(b) due to the extremely over-prediction.

In order to improve the accuracy of the prediction, we changed a constitutive equation of wall friction force to that for separated flow model as a trial. Fig. 12(a) and (b) show the results when interfacial friction correlation by TRAC-PF1/MOD1 and RELAP5/MOD3 was used. The agreement becomes better in comparison with that in Fig. 11(a) and (b), and in Fig. 12(a) and (b) calculation by the combination of TRAC-PF1/MOD1 code for interfacial friction and separated flow model for wall friction gives the best results of within ±20% except for annular flow data at $j_L = 0.2$ m/s.

Fig. 13(a)–(d) show similar comparisons against annular flow data when correlations of Fukano and Furukawa, Henstock and Hanratty, Moeck and Stachiewitz, Wallis were used as the constitutive equation of the interfacial friction force. In these calculations, as a constitutive equation of wall friction force, separated flow model was used again because of its excellent predictability.

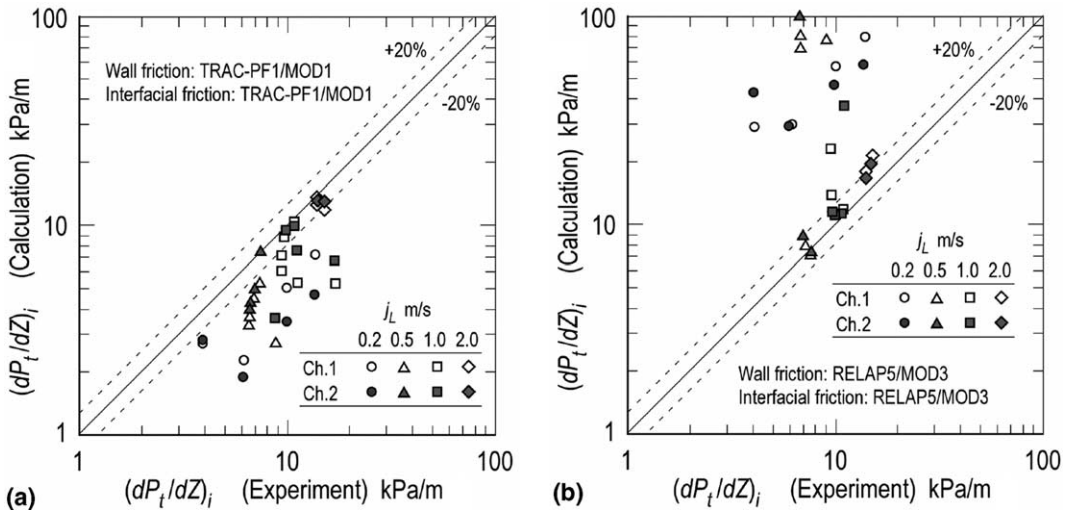

Fig. 11. Comparison of pressure gradient between experiment and calculation: (a) TRAC-PF1/MOD1 correlation and (b) RELAP5/MOD3 correlation.

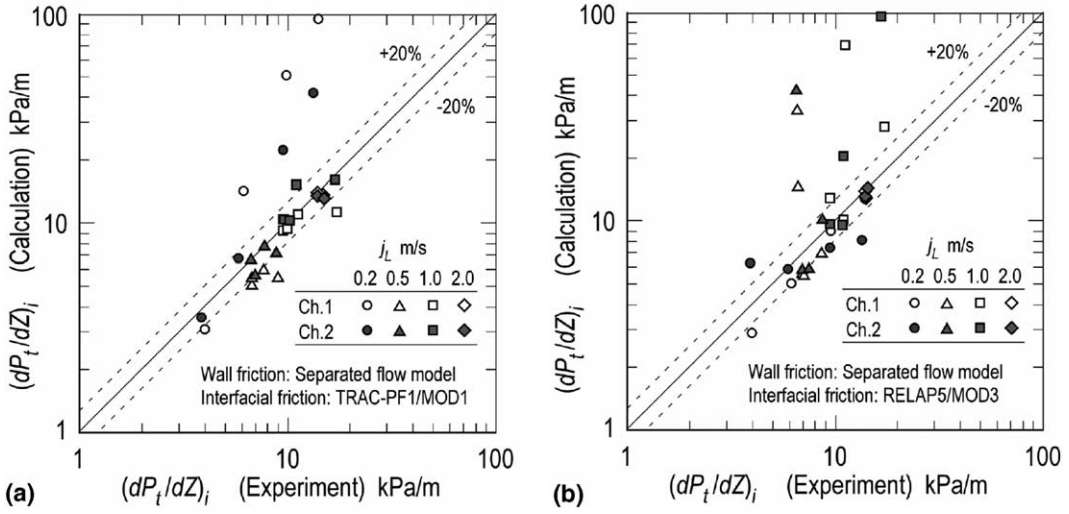

Fig. 12. Comparison of pressure gradient between experiment and calculation when separated flow model is used in the wall friction calculation: (a) TRAC-PF1/MOD1 with separated flow model and (b) RELAP5/MOD3 with separated flow model.

It is found that the agreements for four cases are not bad except for case of Henstock and Hanratty's correlation. For cases of Fukano and Furukawa's and Wallis' correlations, the agreement is better and within ±20%.

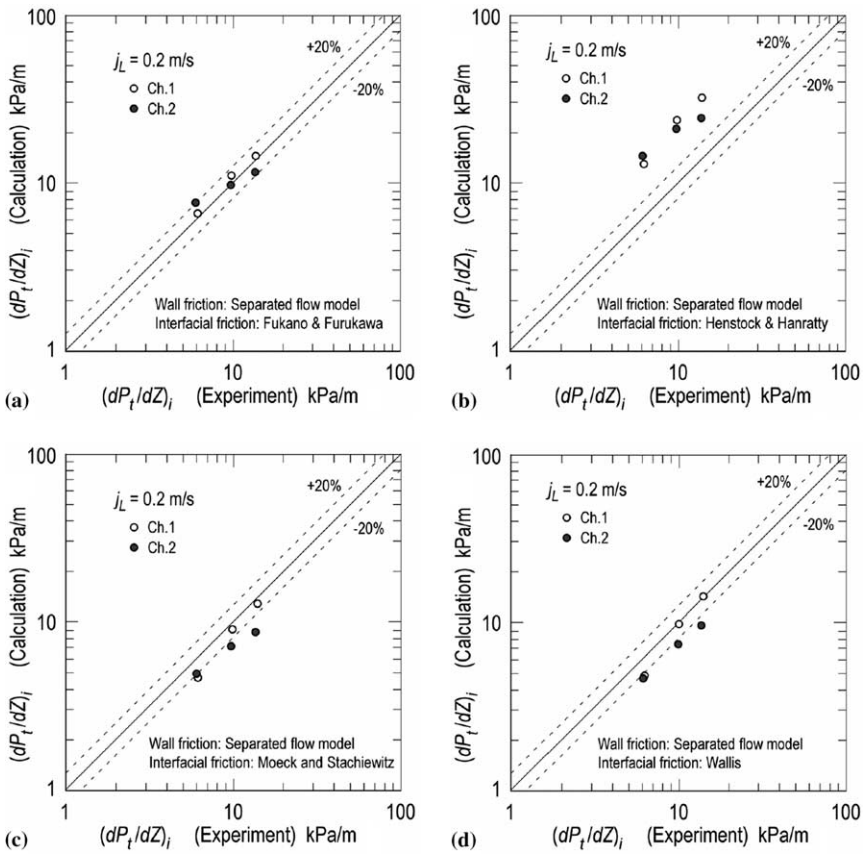

Fig. 13. Comparison of pressure gradient between experiment and calculations for annular flow regime: (a) Fukano and Furukawa's correlation, (b) Henstock and Hanratty's correlation, (c) Moeck and Stachiewitz's correlation and (d) Wallis' correlation.

3.4. Taylor bubble velocity in each subchannel

Fig. 14(a)–(c) show Taylor bubble velocity measured in slug or churn flow in each subchannel at $j_L = 0.5$, 1.0 and 2.0 m/s, superficial liquid velocities in the whole channel. The ordinate indicates the Taylor bubble velocity measured in the subchannels, u_{Gi}, and the abscissa indicates the superficial gas velocity in the whole channel, j_G. The averaged velocity between Ch. 1A and Ch. 1B is plotted as the velocity in Ch. 1, the average velocity among Ch. 2A and Ch. 2B in Ch. 2. u_{Gi} increases with j_G, and the velocity is always faster in Ch. 1 than Ch. 2, irrespective of flow rates conditions. This demonstrates that relatively small cell Taylor bubbles in each subchannel appeared and the effects of the velocity in the neighboring subchannels were small. The large shroud Taylor bubbles occupying all the subchannels, observed in stagnant water test (Venkateswararao et al., 1982), did not emerge in the present experiments. Concerning the data asterisked, comments are given in the next paragraph.

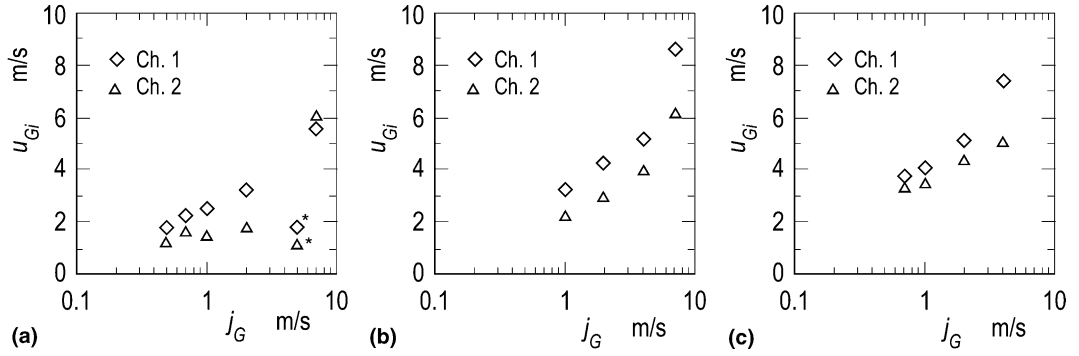

Fig. 14. Taylor bubble velocity in each subchannel against superficial gas velocity in the whole channel: (a) $j_L = 0.5$ m/s, (b) $j_L = 1.0$ m/s and (c) $j_L = 2.0$ m/s.

Fig. 15(a)–(c) shows a plot of u_{Gi} against the total superficial velocity in each subchannel, j_{Ti} ($=j_{Gi}+j_{Li}$), instead of j_G. By taking j_{Ti} as the abscissa, we found that the velocity of both subchannels approaches each other.

The Taylor bubble velocity data are compared with the calculations also in Fig. 15(a)–(c). The solid line is the calculated result by the following Nicklin et al. (1962) type correlation:

$$u_{Gi} = 1.2 j_{Ti} + U_{Ti}, \tag{13}$$

where U_{Ti} is the terminal velocity of Taylor bubble in a stagnant water in Ch. i. In this calculation, we tried to evaluate U_{Ti} using the three kinds of methods shown below:

$$U_{Ti} = 0.35\sqrt{gD_{hi}} \quad \text{(Nicklin et al., 1962)}, \tag{14}$$

$$U_{Ti} = 0.35\sqrt{gD_{ei}} \quad \text{(Sadatomi et al., 1982)}, \tag{15}$$

$$U_{Ti} = Fr_i\sqrt{gD_{hi}(\rho_L - \rho_G)/\rho_L} \quad \text{(White and Beardmore, 1962)}, \tag{16}$$

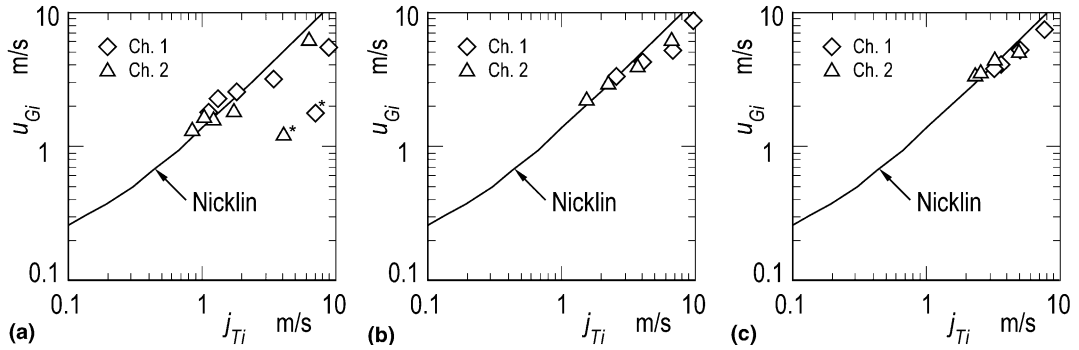

Fig. 15. Taylor bubble velocity in each subchannel against total superficial velocity in each subchannel: (a) $j_L = 0.5$ m/s, (b) $j_L = 1.0$ m/s and (c) $j_L = 2.0$ m/s.

where D_{hi} is the hydraulic equivalent diameter of Ch. i, D_{ei} is the equi-periphery diameter of Ch. i defined as

$$D_{ei} = \frac{\text{wetted perimeter of Ch. } i}{\pi}, \tag{17}$$

which is proposed by Sadatomi et al. (1982). In Eq. (16), Fr_i is the Froude number, determined from a chart by White and Beardmore (1962) using the following two parameters,

$$Eo_i = (\rho_L - \rho_G) g D_{hi}^2/\sigma, \quad M = g\mu_L^4(\rho_L - \rho_G)/(\rho_L^2\sigma^3). \tag{18}$$

In this equation, Eo_i and M are referred to as Eötvös number and Morton number. In addition, g is the acceleration due to gravity and σ the surface tension. Under the present experimental condition, the values of Fr_{Di} are 0.29 and 0.25 for Ch. 1 and Ch. 2. Calculated values of u_{Gi} by Eq. (10) together with Eqs. (14)–(16) showed that u_{Gi} values are nearly the same irrespective of U_{Ti} equations. Consequently, the calculated result by Eq. (13) with (14) alone is shown in Fig. 15(a)–(c), as representative. The data agree well with calculations, except for the data asterisked, which was taken in a highly agitated churn flow. Thus, we can conclude that the Taylor bubble velocity in slug flow in each subchannel in a multi-subchannel system can be estimated from an empirical correlation developed for a simpler channel if j_{Ti} in each subchannel is known.

A time series of signal from the needle contact probes allows us to obtain the data on the length of the Taylor bubble and the slug pitch in each subchannel because u_{Gi} was measured in advance. These obtained data are shown in Appendix A.

3.5. Equilibrium void fraction distribution

As mentioned in Introduction, an accurate evaluation of an equilibrium void fraction distribution is essential to describe the void drift phenomena with Eq. (1), the void settling model. Unfortunately, however, the void fraction in each subchannel was not measured in the present experiments. Instead, the void fraction was determined from the measured data on the flow rates of both phases in this study. In reality, the void fraction in each subchannel, ε_1 or ε_2, was evaluated by the following procedures: (1) Volumetric fluxes of each phase in Ch. 1 and Ch. 2, j_{k1}, j_{k2}, were calculated from the data on the flow rate ratio, Q_{k1}/Q_k with continuity equations for the respective phases; (2) The subchannel void fraction, say ε_1, was calculated by substituting j_{G1} and j_{L1} into Chisholm's void fraction correlation (1973). According to our previous studies on a subchannel void fraction in a channel consisting of two subchannels (Sadatomi et al., 1994; Sadatomi et al., 1996a), the validity of the above procedures was confirmed with the measured subchannel void fraction. So, the validity to the present 2×3 rod bundle channel was checked with the measured data of Taylor bubble velocity in each subchannel in slug flow, $u_{Gi,exp}$. That is, the subchannel void fraction determined from the following relation, $\varepsilon_{i,exp}$,

$$\varepsilon_{i,exp} = \frac{j_{Gi}}{u_{Gi,exp}} \tag{19}$$

by substituting measured data on $u_{Gi,exp}$ and j_{Gi}, superficial gas velocity in Ch. i, was compared with that calculated by Chisholm's correlation:

$$\varepsilon_i = \beta_i \left[\beta_i + \frac{1-\beta_i}{\sqrt{1-\beta_i(1-\rho_G/\rho_L)}} \right]^{-1}, \tag{20}$$

where β_i is the gas volumetric flow fraction,

$$\beta_i = \frac{j_{Gi}}{j_{Gi} + j_{Li}}. \tag{21}$$

Fig. 16(a) and (b) show the results at $j_L = 0.5$ m/s and 2.0 m/s. The void fraction calculated by Chisholm's correlation agrees with $\varepsilon_{i,exp}$, within ±20%, except for highly agitated churn flow region at $\varepsilon_{i,exp} > 0.7$. Because the velocity of Taylor bubble in slug flow is not necessarily the same as that of tiny bubbles contained in the liquid slug behind the Taylor bubble, the void fraction from Eq. (19) is an approximation. However, the approximation must be justified because the total volume of the tiny bubbles is much smaller than that of large Taylor bubble. According to Sadatomi et al.'s study (1982) for a vertical two-phase flow in non-circular channels, the void fraction determined from Eq. (19) and Taylor bubble velocity data agreed with that measured with a quick-closing valve method within ±5% for various slug or churn flows. Furthermore, the Taylor bubble velocity $u_{Gi,exp}$ measured at $\varepsilon_{i,exp} > 0.7$ is not necessarily the mean gas velocity, thus $\varepsilon_{i,exp}$ obtained from the measured $u_{Gi,exp}$ is different from the actual mean void fraction. Taking these facts into consideration, we conclude that Chisholm's void fraction correlation can predict the subchannel void fraction in the present 2×3 rod bundle channel within ±20% at $\varepsilon_{i,exp} < 0.7$, if the flow rates of both phases in the corresponding subchannel are known.

As mentioned above, Chisholm's void fraction correlation may have an error of ±20% for prediction of the subchannel void fraction, ε_i, in the present channel. However, it seems interesting that the subchannel void fraction, ε_i, calculated from Eq. (20) is compared with bundle mean void fraction defined as

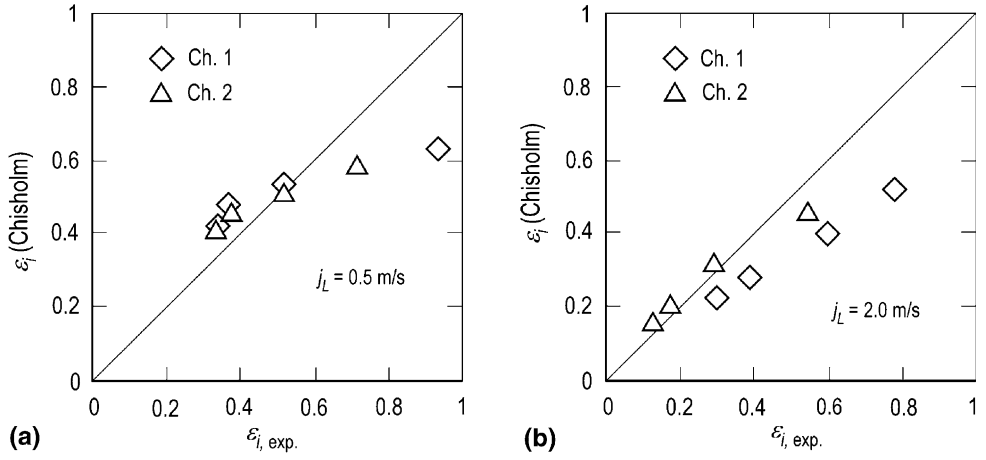

Fig. 16. Comparison of void fraction in each subchannel between calculation by Chisholm's correlation and $\varepsilon_{i,exp}$ by Eq. (16): (a) $j_L = 0.5$ m/s and (b) $j_L = 2.0$ m/s.

$$\varepsilon_{\text{ave}} = \frac{2A_1\varepsilon_1 + 4A_2\varepsilon_2}{2A_1 + 4A_2}. \tag{22}$$

In Eq. (22), ε_1 and ε_2, are calculated from Eq. (20) by substituting the measured data on the superficial velocities of both phases in the corresponding subchannels. A result of comparison between the subchannel void fraction, ε_i, and the bundle mean void fraction calculated is shown in Fig. 17. The data are labeled according to the superficial liquid velocity in the whole channel, j_L, and the subchannel. The solid and broken curves are the subchannel void fractions calculated from the Carlucci et al.'s (2004) correlation mentioned in the next paragraph. The trends of the subchannel void fractions data against the bundle average void fraction are similar irrespective of j_L. In slug or churn flow regime at about $0.2 < \varepsilon_{\text{ave}} < 0.8$, the void fraction in Ch. 1 is higher than that in the whole channel, while the void fraction in Ch. 2 lower, because of higher superficial gas velocity in Ch. 1 than Ch. 2. In addition, it is interesting that the difference of the subchannel void fractions increases a little with j_L. In bubble and annular flow regimes at about $\varepsilon_{\text{ave}} < 0.2$ and $\varepsilon_{\text{ave}} > 0.8$, on the other side, the void fractions in both subchannels are nearly the same. From these results, we can conclude that there is a void fraction difference between Ch. 1 and Ch. 2 in the present channel even in equilibrium flows, especially in slug or churn flow.

A few models (Lahey et al., 1972; Rowe et al., 1990; Carlucci et al., 2004) have been proposed to evaluate the void fraction distribution in a hydraulically equilibrium flow. In what follows, we will examine these models against the present data on the equilibrium void fraction distribution. Firstly, we examine the following Carlucci et al.'s correlation (2004):

$$\varepsilon_i = \varepsilon_{\text{ave}} + KF_{\text{G.P}}\varepsilon_{\text{ave}}(1 - \varepsilon_{\text{ave}})\left(1 - \frac{D_h}{D_{hi}}\right), \tag{23}$$

where K is the coefficient, $F_{\text{G.P}}$ the mass flux and pressure-dependent factor, D_{hi} and D_h the hydraulic equivalent diameter of ith subchannel and that of bundle average, respectively. This correlation was originally proposed by Rowe et al. (1990) and modified to take account of the effects

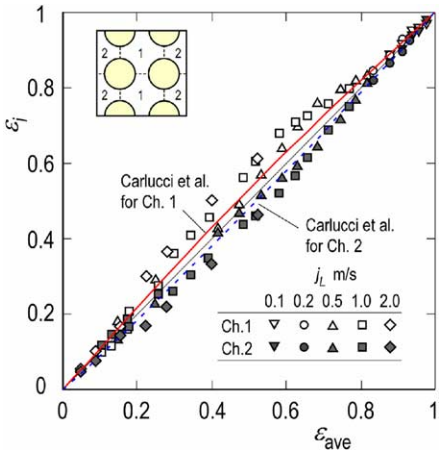

Fig. 17. Comparison of subchannel void fraction with bundle mean void fraction and examination of Carlucci et al.'s correlation.

of mass flux and system pressure with the factor, $F_{G,P}$. The coefficient, K, was determined to be 0.85 based on the flow distribution data obtained by Sterner and Lahey (1983) for air–water mixture flow in a 2×2 rod bundle channel in void fraction range of 0.2–0.6 and at two mass fluxes of 450 and 900 kg/m^{2}s. Fig. 17 shows again an examination of Carlucci et al.'s correlation, solid and broken curves for Ch. 1 and Ch. 2, against the present void distribution data. Single curve is drawn for each subchannel because the factor, $F_{G,P}$, reduced to be unity for all the flow conditions in the present experiments. Eq. (23) agrees well with the present data in bubble flow and annular flow. In slug or churn flow, on the other hand, Eq. (23) underestimates and overestimates the subchannel void fraction of Ch. 1 and Ch. 2, respectively. Therefore, there is room for improvement of the Carlucci et al.'s model.

Another examination is conducted for Lahey et al.'s model (1972). Lahey et al. (1972) derived the following equation based on Levy's (1963) model to describe a relation between the equilibrium void and the mass flux distributions in adjacent subchannels.

$$\frac{(\varepsilon_i - \varepsilon_j)_{EQ}}{\varepsilon_{ave}} = \frac{(\dot{m}_i - \dot{m}_j)_{EQ}}{\dot{m}_{ave}}, \tag{24}$$

where $(\dot{m}_1 - \dot{m}_2)_{EQ}$ is the difference in mass flux between adjacent subchannels in an equilibrium flow, $\dot{m}_{ave}$ the bundle average mass flux. Since Eq. (24) is widely used to predict the equilibrium void fraction distribution (e.g., Kazimi and Kelly, 1983; Tapucu et al., 1994), it is a matter of great importance to test it against the present data. Fig. 18 shows a relationship between $(\varepsilon_1 - \varepsilon_2)_{EQ}/\varepsilon_{ave}$ and $(\dot{m}_1 - \dot{m}_2)_{EQ}/\dot{m}_{ave}$ for the present data at $j_L = 1.0$ m/s and Sterner and Lahey's data (1983) at $\dot{m} = 450$ and 900 kg/m^{2}s in a 2×2 rod bundle channel. The results of both the present and Sterner and Lahey's data do not support Eq. (21), Lahey et al.'s model. A similar result has been noted in the two-subchannel experiments by Sadatomi et al. (1994).

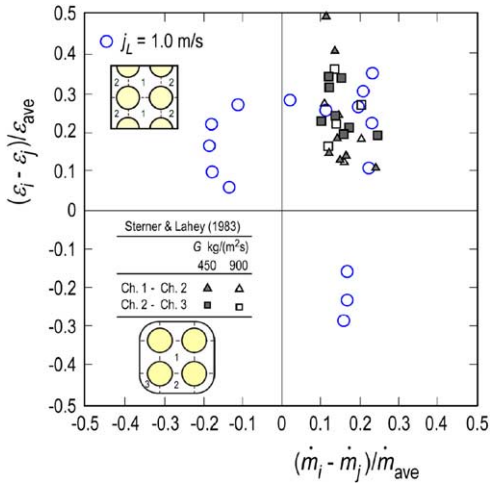

Fig. 18. Relation between void fraction distribution and mass flux distribution in equilibrium flows in 2×3 rod bundle channel at $j_L = 1.0$ m/s and in 2×2 rod channel (Sterner and Lahey, 1983) at $\dot{m} = 450$ and 900 kg/m^{2}s.

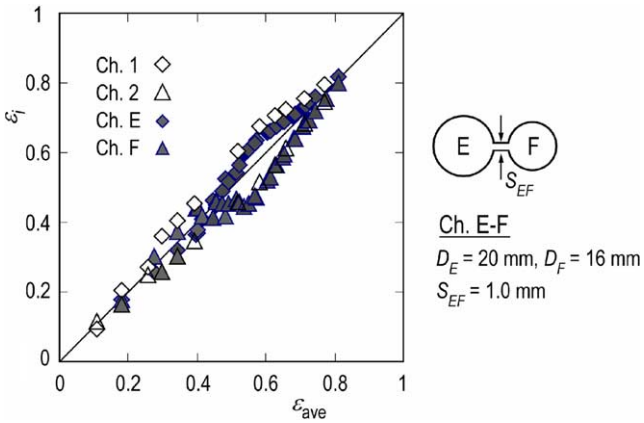

Fig. 19. Comparison of void fraction in each subchannel between in two-subchannel system and in the present multi-subchannel system ($j_L = 1.0$ m/s).

Fig. 19 shows a comparison of the subchannel void fraction in the present 2×3 rod bundle channel with that in two-subchannel system, referred to Ch. E–F in our laboratory (Sadatomi et al., 1994), at $j_L = 1.0$ m/s. The ratio of cross-sectional areas between larger and smaller is similar in these channels, i.e., $A_E/A_F = 1.56$ and $A_1/A_2 = 1.41$. The trend of the data in Ch. E–F is quite similar to that in the 2×3 rod bundle channel. This suggests that a lot of experimental information so far on a two-subchannel system are usable for understanding phenomena in a multi-subchannel system.

4. Conclusions

In order to obtain data to validate a subchannel analysis code, we made a new vertical test channel with six subchannels around 2×3 square array rods, i.e., 2×3 rod bundle channel. The experiments were made in various iso-thermal single-phase water and two-phase air–water flows under the hydrodynamic equilibrium flow conditions. In the experiments, data on flow distribution, axial pressure drop and Taylor bubble velocity in each subchannel were obtained. From the results of the experiments and the analysis of the data, we found the following main findings:

- The single-phase water flow distribution data could be predicted well with Sato et al.'s method (1983).
- A similar trend of the two-phase flow distribution data was noted between the present multi-subchannel system and a two-subchannel system, i.e., superficial gas velocity was higher in the larger subchannel than the smaller subchannel, especially in slug or churn flow regime.
- The single-phase friction factor data in each subchannel could be predicted well with Sadatomi et al.'s (1982) equation for non-circular channels.
- The two-phase pressure drop data agreed well with calculations from a simple, one-dimensional, one-pressure two-fluid model, when appropriate equations of wall friction and interfacial friction forces were used. A separated flow model (Chierici et al., 1974; Ali et al., 1993) was

appropriate for the wall friction force. TRAC-PF1/MOD1 (1988) code correlation in bubble, slug and churn flow regimes, and Fukano and Furukawa's (1998), Wallis' (1969, 1970) and Moeck and Stachiewitz's (1970) correlations in annular flow regime were appropriate for the interfacial friction force.

- The Taylor bubble velocity becomes higher in the larger subchannel than the smaller subchannel. This demonstrates that relatively small cell Taylor bubbles appeared in each subchannel. The cell Taylor bubble velocity can be well predicted from a Nicklin et al.'s (1962) type correlation by substituting the measured flow rates of both phases in the respective subchannels. The large shroud Taylor bubble occupying all the subchannels, seen in a stagnant water test (Venkateswararao et al., 1982), did not emerge in the present experiments.
- The subchannel void fraction can be estimated from Chisholm's correlation (1973) by substituting flow rates of both phases in the respective subchannels.
- For prediction of the subchannel void fraction under the equilibrium flow conditions, Carlucci et al.'s correlation (2004) was useful in bubble flow and annular flow regimes. In slug and churn flows, their correlation underestimated and overestimated the subchannel void fractions of larger and smaller subchannels, respectively. In addition, Lahey et al.'s model (1972) was ineffective to predict the present subchannel void fraction data.
- The similarity in the subchannel void fraction distribution between the present multi-subchannel and a two-subchannel system suggests that much of the knowledge obtained so far in a two-subchannel system must be useful to understand phenomena in a multi-subchannel system.

Acknowledgments

The authors wish to express their gratitude to Messrs. A. Fukumoto, K. Omori, S.T. Kuno, Y. Muraoka, Y. Minesaki, who were then students at Kumamoto University, for their help with the experiments, and to the Institute of Applied Energy (IAE), Ministry of Economy, Trade and Industry (METI), Japan, for financial support to this study.

Appendix A

In slug or churn flows, the length of the Taylor bubble as well as the slug pitch defined as the total length of a Taylor bubble and a liquid slug are the important parameters for modeling the turbulent mixing between the subchannels (Kawahara et al., 1997; Sadatomi et al., 2004). These parameters are also important for developing and/or examining the constitutive equations of interfacial transfers needed in a multi-fluid model. Fig. 20(a)–(c) show the slug pitch measured in each subchannel at $j_L = 0.5$, 1.0 and 2.0 m/s, superficial liquid velocities in the whole channel. The ordinate is the pitch to hydraulic diameter ratio in each subchannel, l_i/D_{hi}, while the abscissa the superficial gas velocity in the subchannel, j_{Gi}. The general trend of l_i/D_{hi} is as follows:

- The l_i/D_{hi} value is infinity in bubble flow because of no Taylor bubble. With increasing of j_{Gi} Taylor bubble emerges, and l_i/D_{hi} drastically decreased at a transition region from bubble flow to slug flow.

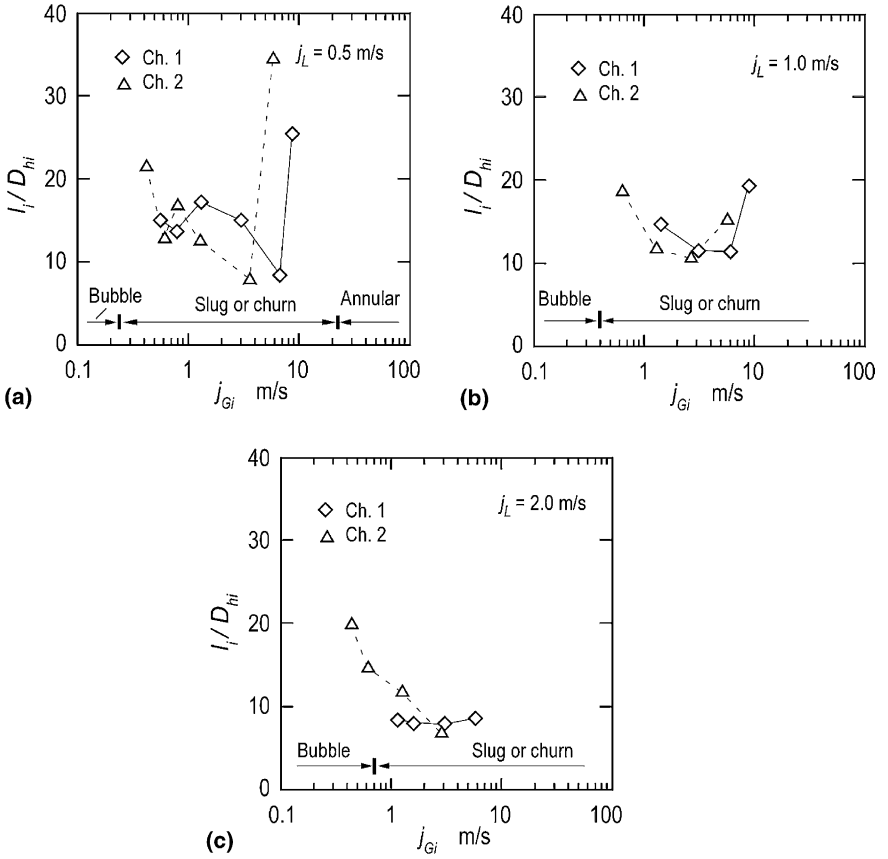

Fig. 20. Taylor bubble pitch to subchannel hydraulic diameter ratio against the superficial gas velocity in each subchannel: (a) $j_L = 0.5$ m/s, (b) $j_L = 1.0$ m/s and (c) $j_L = 2.0$ m/s.

- In slug or churn flow, the trends are different depending on j_L. At $j_L = 0.5$ m/s, l_i/D_{hi} gradually went up with j_{Gi} and then went down at $j_{G1} = 1.3$ m/s for Ch. 1 and $j_{G2} = 0.8$ m/s for Ch. 2, because the flow proceeds to a highly agitated churn flow. At $j_L = 1.0$ m/s and $j_L = 2.0$ m/s, however, such an up and down were not observed.
- At a transition from churn flow to annular flow, l_i/D_{hi} steeply increased with j_{Gi} because liquid slugs disappeared.

These trends are quite similar to that reported by Sato et al. (1981) for flows in a vertical 26 mm I.D. circular pipe.

Fig. 21(a)–(c) show the Taylor bubble length measured in each subchannel at the same flow conditions as Fig. 20(a)–(c). The ordinate is the bubble length to the slug pitch ratio in each subchannel, l_{Gi}/l_i, while the abscissa the void fraction in the subchannel, ε_{Gi}. The solid line is the calculated result by the following Sato et al. (1981) correlation:

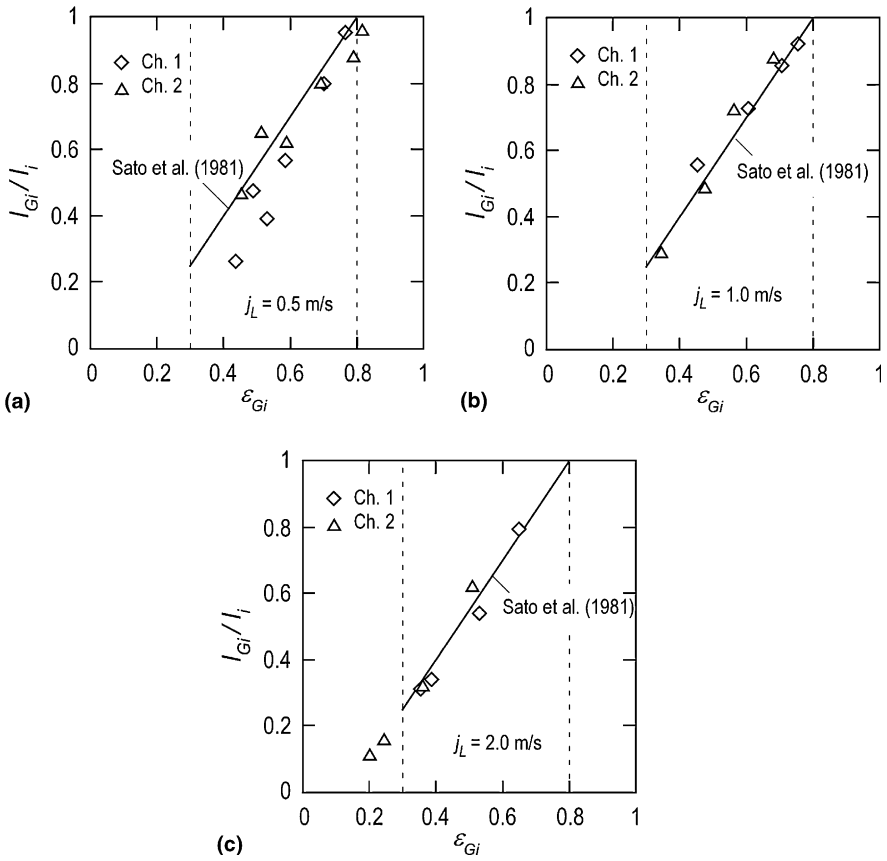

Fig. 21. Taylor bubble length to the pitch ratio against the superficial gas velocity in each subchannel: (a) $j_L = 0.5$ m/s, (b) $j_L = 1.0$ m/s and (c) $j_L = 2.0$ m/s.

$$\frac{l_{Gi}}{l_i} = 1.5\varepsilon_{Gi} - 0.2, \tag{A.1}$$

which is applicable to the circular pipe flow in a void fraction range of $0.3 < \varepsilon_{Gi} < 0.8$ (Sato et al., 1981). The present data on Ch. 1 and Ch. 2 agree well with the calculations. Thus, we can conclude that the Taylor bubble length in each subchannel in a multi-subchannel system can be estimated from the empirical correlation developed for a circular pipe if the void fraction (or gas and liquid volume flow rates) in each subchannel are known.

References

Ali, M., Sadatomi, M., Kawaji, M., 1993. Adiabatic two-phase flow in narrow channels between two flat plates. Can. J. Chem. Engng. 71, 657–666.

Carlson, K.E., Riemke, R.A., Rouhani, S.Z., Shumaway, R.W., Weaver, W.L., 1990. RELAP5/MOD3 Code Manual Volume IV: Models and Correlations. NUREG/CR-5533, EGG-2596.

Carlucci, L.N., Hammouda, N., Rowe, D.S., 2004. Two-phase turbulent mixing and buoyancy drift in rod bundles. Nucl. Engng. Des. 227, 65–84.

Chierici, G.L., Ciucci, G.M., Sclocchi, G., 1974. Two-phase vertical flow in oil wells—Prediction of pressure drop. J. Petroleum Tech. 26, 927–938.

Chisholm, D., 1973. Void fraction during two-phase flow. J. Mech. Eng. Sci. 15, 235–236.

Fukano, T., Furukawa, T., 1998. Prediction of the effects of liquid viscosity on interfacial shear stress and frictional pressure drop in vertical upward gas–liquid annular flow. Int. J. Multiphase Flow 24, 587–603.

Golan, L.P., Stenning, A.H., 1969. Two-phase vertical flow maps. In: Proceedings of Symposium on Fluid Mechanics and Measurements in Two-Phase Flow Systems, Leeds University, Paper No. 14, pp. 24–25.

Gonzalez-Santalo, J.M., Griffith, P., 1972. Two-phase flow mixing in rod bundle subchannel. ASME Paper 72-WA/NE-19.

Henstock, W.H., Hanratty, T.J., 1976. The interfacial drag and the height of the wall layer in annular flows. AIChE J. 26, 990–1000.

Ishii, M., Grolmes, M.A., 1975. Inception criteria for droplet entrainment in two-phase concurrent film flow. AIChE J. 21, 308–318.

Kawahara, A., Sadatomi, M., 2000a, Modeling of void diffusion coefficient in a two-phase subchannel flow. In: Proceedings of 4th JSME-KSME Thermal Engineering Conference 2, Kobe, Japan, pp. 611–616.

Kawahara, A., Sadatomi, M., Iwamoto, K., 2000b. Calculation of two-phase flow redistribution due to void drift in two-interconnected subchannels by a two-fluid model. In: Proceedings of Second Japan-Korea Symposium on Nuclear Thermal Hydraulics and Safety NTHAS2, Fukuoka, Japan, pp. 719–725.

Kawahara, A., Sadatomi, M., Tomino, T., Sato, Y., 2000c. Prediction of turbulent mixing rates of both gas and liquid phases between adjacent subchannels in a two-phase slug-churn flow. Nucl. Engng. Des. 202, 27–38.

Kawahara, A., Sato, Y., Sadatomi, M., 1997. The turbulent mixing rate and the fluctuations of static pressure difference between adjacent subchannels in a two-phase subchannel flow. Nucl. Engng. Des. 175, 97–106.

Kazimi, M.S., Kelly, J.E., 1983. Formulation of a two-fluid model for mixing in LWR bundles. In: Proceedings of the 2nd International Topical Meeting on Nuclear Reactor Thermal Hydraulics, Santa Barbara, California, USA, pp. 433–439.

Lahey Jr., R.T., Moody, F.J., 1993. The Thermal-Hydraulics of a Boiling Water Nuclear Reactor, second ed. ANS, La Grange Park pp. 168–184.

Lahey Jr., R.T., Shiralkar, B.S., Radcliffe, D.W., Polomik, E.E., 1972. Out-of-pipe sub-channel measurements in a nine rod bundle for water at 1000 psia. In: Hetsroni, G. et al. (Eds.), Progress in Heat and Mass Transfer, 6, Pergamon Press, London, pp. 345–363.

Levy, S., 1963. Prediction of two-phase pressure drop and density distribution from mixing length theory. Trans. ASME J. Heat Transfer 85, 137–152.

Lies, D.R., Spore, J.W., Knight, T.D., Nelson, R.A., Cappiello, M.W., Pasamehmetoglu, K.O., Mahaffy, J.H., Guffee, L.A., Stumpf, H.J., Dotson, P.J., Steinke, R.G., Shire, P.R., Greiner, S.E., Sherwood, K.B., 1988. TRAC-PF1/MOD1 Correlations and Models. NUREG/GR-5069, LA-11208-MS.

Mishima, K., Ishii, M., 1984. Flow regime transition criteria for upward two-phase flow in vertical tubes. Int. J. Heat Mass Transfer 27, 723–737.

Moeck, E.O., Stachiewitz, J.W., 1970. A droplet interchange model for annular-dispersed two-phase flow. Int. J. Heat Mass Transfer 15, 637–653.

Nicklin, D.J., Wilkes, J.O., Davidson, J.F., 1962. Two-phase flow in vertical pipes. Trans. Inst. Chem. Engrs. 40, 61–68.

Ninokata, H., Aritomi, M., Anegawa, T., Sato, Y., Sadatomi, M., Mishima, K., Nishida, K., Yamamoto, Y., Morooka, S., Yabushita, Y., Sou, A., Kamo, H., Kusuno, S., 1997. Development of the NASCA code for prediction of transient BT and post BT phenomena in BWR rod bundles. In: Proceedings of 4th International Seminar on Subchannel Analysis, Tokyo, Japan, pp. 231–265.

Rehme, K., 1973. Simple method of predicting friction factors of turbulent flow in non-circular channels. Int. J. Heat Mass Transfer 16, 933–950.

Rowe, D.S., Angle, C.W., 1969. Crossflow mixing between parallel flow channels during boiling. Part III: Effect of spacers on mixing between two channels. Battelle Northwest Laboratory BNWL-371 Part 3.

Rowe, D.S., Macduff, R.B., Collingham, R.E., 1990. Thermal hydraulic subchannel model based on void-drift. Heat Transfer 1, 401–406.

Rudzinski, K.F., Singh, K., St. Pierre, C.C., 1972. Turbulent mixing for air–water two-phase flows in simulated rod bundle geometries. Can. J. Chem. Engng. 50, 297–299.

Sadatomi, M., Kawahara, A., Kano, K., Sumi, Y., 2004. Single- and two-phase turbulent mixing rate between adjacent subchannels in a vertical 2×3 rod array channel. Int. J. Multiphase Flow 30, 481–498.

Sadatomi, M., Kawahara, A., Sato, Y., 1994. Flow redistribution due to void drift in two-phase flow in a multiple channel consisting of two subchannels. Nucl. Engng. Des. 148, 463–474.

Sadatomi, M., Kawahara, A., Sato, Y., 1995. Turbulent mixing of both gas and liquid phases between subchannels in two-phase hydrodynamic equilibrium flows. In: Celeta, G.P., Shah, R.K. (Eds.), Proceedings of International Symposium on Two-Phase Flow Modelling and Experimentation 1995 1, Rome, pp. 403–409.

Sadatomi, M., Kawahara, A., Sato, Y., 1996a. Axial variation of void fraction in a hydraulically non-equilibrium two-phase flow in a vertical multiple channel. In: Proceedings of the 3rd KSME-JSME Thermal Engineering Conference 1, Kyongju, Korea, 339–344.

Sadatomi, M., Kawahara, A., Sato, Y., 1996b. Prediction of the single-phase turbulent mixing rate between two parallel subchannels using a subchannel geometry factor. Nucl. Engng. Des. 162, 245–256.

Sadatomi, M., Kawahara, A., Sato, Y., 1997. Treatment of two-phase turbulent mixing, void drift and diversion cross-flow in a hydraulically non-equilibrium subchannel flow. In: Proceedings of 4th International Seminar on Subchannel Analysis, Tokyo, Japan, pp. 87–104.

Sadatomi, M., Sato, Y., Saruwatari, S., 1982. Two-phase flow in vertical noncircular channels. Int. J. Multiphase Flow 8, 641–655.

Sato, Y., Sadatomi, M., 1988. Two-phase gas–liquid flow distributions in multiple channels. In: Proceedings of JAPAN-US Seminar on Two-Phase Flow Dynamics, Ohtsu, Japan, E4, pp. 1–10.

Sato, Y., Sadatomi, M., Kanesaki, K., 1981. Study on slug flow characteristics in vertical two-phase flow. In: Proceedings of JSME No. 818-1, pp. 98–100 (in Japanese).

Sato, Y., Sadatomi, M., Kawahara, A., 1996. A proposal for treatment of turbulent mixing in a two-phase subchannel flow. Chem. Engng. Commun. 141&142, 399–413.

Sato, Y., Sadatomi, M., Mine, T., 1983. Flow distribution and pressure drop in a flow parallel to rod bundle. Trans. JSME part-B 49, 1135–1142 (in Japanese).

Sato, Y., Sadatomi, M., Tsukashima, H., 1987. Two-phase flow characteristics in interconnected subchannels with different cross-sectional areas. In: Proceedings of ASME-JSME Thermal Engineering Joint Conference, Honolulu, Hawaii, USA, pp. 389–395.

Sterner, R.W., Lahey Jr., R.T., 1983. Air/water subchannel measurements of the equilibrium quality and mass-flux distribution in a rod bundle. US DOE Report, NUREG/CR-3373.

Taitel, Y., Barnea, D., Duckler, A.E., 1980. Modeling of flow pattern transition for steady upward gas–liquid flow in a vertical tubes. AIChE J. 26, 345–354.

Tapucu, A., Geçkinli, M., Troche, N., Girard, R., 1988. Experimental investigation of mass exchanges between two laterally interconnected two-phase flow. Nucl. Engng. Des. 105, 295–312.

Tapucu, A., Teyssedou, A., Geçkinli, M., Merilo, M., 1990. Axial pressure distribution in two laterally interconnected channels with blockages. Int. J. Multiphase Flow 16, 461–479.

Tapucu, A., Teyssedou, A., Tye, P., Troche, N., 1994. The effect of turbulent mixing models on the predictions of subchannels codes. Nucl. Engng. Des. 149, 221–231.

Teyssedou, A., Tapucu, A., Geçkinli, M., Merilo, M., 1989a. Axial void distribution in two laterally interconnected channels with blockages. Int. J. Multiphase Flow 15, 65–79.

Teyssedou, A., Tapucu, A., Geçkinli, M., Merilo, M., 1989b. Axial mass flow distribution in two laterally interconnected channels with blockages. Int. J. Multiphase Flow 15, 605–626.

Venkateswararao, P., Semiat, R., Dukler, A.E., 1982. Flow pattern transition for gas–liquid flow in a vertical rod bundle. Int. J. Multiphase Flow 8, 509–524.

Wallis, G.B., 1969. One-Dimensional Two-Phase Flow. McGraw-Hill Book Co. Inc., New York.

Wallis, G.B., 1970. Annular two-phase plow Part 1: A simple theory. Trans. ASME. J. Basic Engng. 82, 59–72.

White, E.T., Beardmore, R.H., 1962. The velocity of rise of single cylindrical air bubbles through liquids contained in vertical tubes. Chem. Engng. Sci. 17, 351–361.

Yadigaroglu, G., Maganas, A., 1995. Equilibrium quality and mass flux distributions in an adiabatic three-subchannel test section. Heat Transfer Fluid Flow 112, 359–372.